PHYSICAL METALLURGY AND HEAT TREATMENT / МЕТАЛЛОВЕДЕНИЕ И ТЕРМИЧЕСКАЯ ОБРАБОТКА

UDC 621.791.755, 621.785.01
https://doi.org/10.17073/0021-3438-2024-2-16-29

Research article
Научная статья

Structure and mechanical properties of Ti_2AlNb-based alloy welded joints using keyhole plasma arc welding with subsequent heat treatment

S.V. Naumov[1], D.O. Panov[1], R.S. Chernichenko[1], V.S. Sokolovsky[1], G.A. Salishchev[1], E.B. Alekseev[2], S.D. Neulybin[3], D.S. Belinin[3], Yu.D. Shchitsyn[3], V.V. Lukianov[4]

[1] **Belgorod National Research University**
85 Pobedy Str., Belgorod 308015, Russia

[2] **All-Russian Research Institute of Aviation Materials of the National Research Center "Kurchatov Institute"**
17 Radio Str., Moscow 105005, Russia

[3] **Perm National Research Polytechnic University**
29 Komsomolskiy Prosp., Perm 614990, Russia

[4] **NPA "Technopark AT"**
5 bld. 1 Tramvaynaya Str., Ufa 450027, Russia

✉ Stanislav V. Naumov (NaumovStanislav@yandex.ru)

Abstract: Using keyhole plasma arc welding, welded joints of a Ti_2AlNb-based alloy, VTI-4, were obtained, and their structure and mechanical properties were studied. It has been established that the dynamic effect of a keyhole arc had a positive effect on the quality of the welded joint; namely, lack of penetration, porosity, and microcracks were eliminated. The welded joint consisted of a fusion zone (FZ), a heat-affected zone (HAZ), and a base metal (BM). Depending on the phase composition and morphology of the obtained phases, the HAZ can be divided into four zones: HAZ1 with large β-phase grains near the melting line, HAZ2 with large β-phase grains + α_2, HAZ3 with more fragmented β-phase grains retaining more α_2-phase, and HAZ4 with the phase composition β + α_2 + O. Subsequent heat treatment (HT: quenching at 920 °C for 2 h, cooling in air, followed by aging at 800 °C for 6 h, cooling in air) preserved the zone structure of the weld but led to the formation of the O-phase within β-grains. The microhardness of the weld in the zone corresponds to 360±15 $HV_{0.2}$, but after HT, it increased to 382±20 $HV_{0.2}$. The strength properties of the welded joint after HT were above 90 % of the base metal (σ_{ucs} = 1120 MPa, $\sigma_{0.2}$ = 1090 MPa), while elongation to failure is close to the initial condition (δ = 2.1 %).

Keywords: VTI-4 alloy based on orthorhombic titanium aluminide, Ti_2AlNb, keyhole plasma arc welding, weld seam, BSE analysis, EBSD analysis, mechanical properties, microhardness.

Acknowledgments: This work was supported by the Russian Science Foundation (Agreement No. 19-79-30066) using the equipment of BSU Shared Research Facilities "Technologies and Materials ".

For citation: Naumov S.V., Panov D.O., Chernichenko R.S., Sokolovsky V.S., Salishchev G.A., Alekseev E.B., Neulybin S.D., Belinin D.S., Shchitsyn Yu.D., Lukianov V.V. Structure and mechanical properties of Ti_2AlNb-based alloy welded joints using keyhole plasma arc welding with subsequent heat treatment. *Izvestiya. Non-Ferrous Metallurgy*. 2024;30(2):16–29.
https://doi.org/10.17073/0021-3438-2024-2-16-29

Структура и механические свойства сварных соединений из сплава на основе орторомбического алюминида титана, полученных плазменной сваркой проникающей дугой с последующей термической обработкой

С.В. Наумов[1], **Д.О. Панов**[1], **Р.С. Черниченко**[1], **В.С. Соколовский**[1], **Г.А. Салищев**[1], **Е.Б. Алексеев**[2], **С.Д. Неулыбин**[3], **Д.С. Белинин**[3], **Ю.Д. Щицын**[3], **В.В. Лукьянов**[4]

[1] **Белгородский государственный национальный исследовательский университет**
Россия, 308015, г. Белгород, ул. Победы, 85

[2] **Всероссийский научно-исследовательский институт авиационных материалов Национального исследовательского центра «Курчатовский институт»**
Россия, 105005, г. Москва, ул. Радио, 17

[3] **Пермский национальный исследовательский политехнический университет**
Россия, 614990, г. Пермь, Комсомольский пр-т, 29

[4] **НПА «Технопарк АТ»**
Россия, 450027, г. Уфа, ул. Трамвайная, 5, корп. 1

✉ Станислав Валентинович Наумов (NaumovStanislav@yandex.ru)

Аннотация: Методом плазменной сварки проникающей дугой заготовок из сплава ВТИ-4 на основе орторомбического алюминида титана Ti_2AlNb получены сварные соединения и исследованы их структура и механические свойства. Установлено, что динамическое воздействие проникающей дуги оказывает положительное влияние на качество сварного соединения: исключаются непровар, возникновение пористости и микротрещин, а также формируется благоприятная форма корня шва. Обнаружено, что сварное соединение состоит из зоны плавления (ЗП), зоны термического влияния (ЗТВ) и основного металла (ОМ). В зависимости от фазового состава и морфологии фаз ЗТВ можно разделить на 4 области: ЗТВ1 из крупных зерен β-фазы вблизи линии сплавления, ЗТВ2 из крупных зерен β-фазы + α_2, ЗТВ3 с более фрагментированными зернами β-фазы с сохранением большего количества α_2-фазы и ЗТВ4, имеющей фазовый состав β + α_2 + O. Последующая термическая обработка (ТО: закалка при температуре 920 °С с выдержкой 2 ч и охлаждением на воздухе с последующей выдержкой 6 ч при 800 °С и дальнейшим охлаждением на воздухе) обеспечивает сохранение зонной структуры сварного шва, но приводит к формированию во всех зонах внутри β-зерен частиц O-фазы. Микротвердость сварного шва в зоне плавления соответствует 360±15 $HV_{0,2}$, а после ТО она возрастает до 382±20 $HV_{0,2}$. Прочностные свойства сварного соединения после ТО находятся на уровне выше 90 % от показателей исходной кованой заготовки ($\sigma_в$ = 1120 МПа, $\sigma_{0,2}$ = 1090 МПа), а пластичность близка к исходному состоянию (δ = 2,1 %).

Ключевые слова: сплав ВТИ-4 на основе орторомбического алюминида титана, Ti_2AlNb, плазменная сварка проникающей дугой, сварной шов, BSE-анализ, EBSD-анализ, механические свойства, микротвердость.

Благодарности: Работа выполнена при финансовой поддержке РНФ (Соглашение № 19-79-30066) с использованием оборудования Центра коллективного пользования «Технологии и Материалы НИУ “БелГУ”».

Для цитирования: Наумов С.В., Панов Д.О., Черниченко Р.С., Соколовский В.С., Салищев Г.А., Алексеев Е.Б., Неулыбин С.Д., Белинин Д.С., Щицын Ю.Д., Лукьянов В.В. Структура и механические свойства сварных соединений из сплава на основе орторомбического алюминида титана, полученных плазменной сваркой проникающей дугой с последующей термической обработкой. *Известия вузов. Цветная металлургия*. 2024;30(2):16–29.
https://doi.org/10.17073/0021-3438-2024-2-16-29

Introduction

Titanium alloys based on orthorhombic titanium aluminide (Ti_2AlNb alloys) are considered as a potential replacement for Ni-based superalloys in the aerospace industry [1]. The interest in these materials is due to their high creep resistance and burn resistance compared to conventional titanium alloys, allowing their use at temperatures up to 650 °C [2]. Additionally, they have higher ductility and crack resistance compared to γ-TiAl- and α_2-Ti_3Al-based alloys and lower density (ρ = 5÷6 gm/cm^3) compared to Ni-based superalloys [3—6].

One of the main obstacles to the widespread use of Ti_2AlNb alloys is the difficulty in obtaining high-quality weld joints due to low thermal conductivity, high residual stresses, and a cascade of phase transformations during cooling. These characteristics require the selection of welding parameters to achieve the optimal structure of the weld joint for the desired mechanical properties. Technologies for creating non-dismountable joints have been proposed to manufacture high-quality structures, expanding the application range of Ti_2AlNb alloys [7]: tungsten inert gas welding (TIG) [8; 9], diffusion bonding [10; 11], friction stir welding [12; 13], laser beam welding [14—16], electron beam welding [17—19], etc. Among the welding methods for titanium alloys, TIG welding is the most widely used in the industry [20].

Common problems when using TIG welding with Ti_2AlNb alloys include low productivity, porosity of the weld joint, and the formation of a coarse dendritic structure of the β-phase in the fusion zone. Additionally, when welding thick (>4 mm) products, it is necessary to use filler material with a corresponding chemical composition, which requires the manufacturing of such consumables [21]. Moreover, multi-pass welding leads to repeated overheating of the weld joint, resulting in significant grain growth and consequently low ductility. On the other hand, keyhole plasma arc welding (K-PAW) can serve as the most technologically advanced alternative among arc welding methods for obtaining non-dismountable joints, allowing for defect-free welds of titanium alloys over a wide range of thicknesses. This method has not been used to obtain non-dismountable joints from Ti_2AlNb alloys, requiring research on the influence of welding parameters on the quality of the weld joint, its structure, and mechanical properties.

Thus, the aim of this study was to develop K-PAW parameters and determine the influence of the optimal welding regime and subsequent heat treatment on the structure and properties of welded joints made from the VTi-4 alloy based on orthorhombic titanium aluminide (Ti_2AlNb).

Materials and research methods

The study utilized plates made from the VTi-4 alloy, the chemical composition of which is provided below, in at.%:

Ti.. Base
Al 23
Nb 23
V.. 1.4
Zr 0.8
Mo 0.4
Si.. 0.4

The investigated alloy in its initial forged state possesses the following mechanical properties: ultimate tensile strength (σ_{ucs}) = 1230 MPa, yield strength (σ_{ys}) = = 1190 MPa, elongation to failure (δ) = 3.5 %, microhardness 420±15 $HV_{0.2}$.

The microstructure of the initial billet in the form of a hot-rolled plate is shown in Fig. 1. It exhibits large β-grains with a size of 300±50 μm, with globular α_2-phase grains of 10±5 μm located along the grain boundaries. Additionally, uniformly distributed within the volume of the β-grains, there are needle-like ω-phase precipitates with a length of 8±3 μm and a thickness of 1—3 μm.

K-PAW was performed using the PMI-350 AC/DC TL power source (SBI, Austria) on an automated gantry-type console [22]. Fixing plates were welded to the welding locations to secure the workpieces

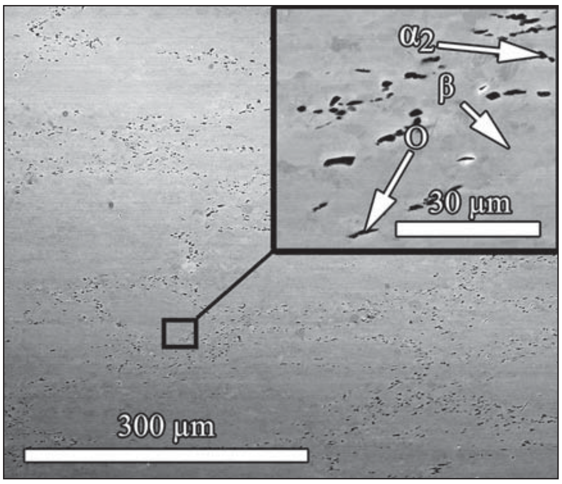

Fig. 1. Microstructure of forged plate of the VTI-4 alloy

Рис. 1. Микроструктура горячекованой плиты из сплава ВТИ-4 in the fixture, allowing for the delivery of shielding gas to the root of the weld joint and ensuring uniform movement of the plasma torch with the shielding block. Samples for K-PAW with dimensions of $50 \times 25 \times 4$ mm were cut from the forged plate. Prior to welding, the entire surface of the samples was ground with abrasive paper with a grain size of 68 μm FEPA P № 220, and the mating surface at the joint was ground with grinding wheels with a grain size of 18 μm FEPA P № 1000.

Welding of 4 mm thick plates made from the VTi-4 alloy was performed end-to-end without gaps or filler material. The melting current required to form a hole at the root of the weld (keyhole) was set at 150—160 A and applied for 0.5 sec. As a result of the melting, the welding process transitions to the keyhole mode, and part of the arc energy is dissipated. The main welding current in this process is reduced to 140—150 A, the arc voltage is 21—22 V, welding speed is 20 m/h, and the current at the end of welding (at the moment of exiting the fixating plates) drops to 15—20 A. Since non-consumable (copper) fixating plates were used, the welding process was completed at minimal currents. The plasma-forming gas flow rate was 3 L/min, the shielding gas flow rate was 3 L/min, and the additional shielding gas flow rate for the shielding block was 8 L/min. Argon grade 5.0 (99.999 % Ar) was used as the plasma-forming gas.

The interaction of the compressed arc with the weld pool occurs in the formed crater cavity.

The magnitude and nature of the distribution of the compressive arc's force impact in the weld pool largely determine the characteristics of the melting front ablation process, molten metal movement, bath retention, and the quality of weld root formation.

Welded joints underwent heat treatment in a split-type folding tube furnace RS80/300/13 ("Nabertherm", Germany) according to the quenching + aging: quenching at a temperature of 920 °C for 2 h followed by air cooling and subsequent aging for 6 h at 800 °C with further air cooling. Prior to loading the samples into the furnace, they were subjected to a 3-cycle argon purging and vacuum evacuation. Heating was performed in an argon atmosphere with excess pressure.

Samples for mechanical testing and microstructural analysis were cut using a Sodick VL400Q wire EDM machine (China). The surfaces of the samples were ground using Struers SiC FEPA P № 220-2000 abrasive materials (from 68 to 10 μm) on Metrotest (Russia), Baipol Metco (India), and LaboPol-5 ("Struers", Denmark) equipment. Subsequent surface polishing was carried out using Struers MD Chem suspension with OP-S NonDry suspension. Samples for further microstructural analysis were cleaned of organic matter, suspension particles, or abrasive in an ultrasonic bath model 3404 ("Sapphire", Russia) with acetone for 15 minutes.

The microstructure was examined using a Q600 3D electron microscope (FEI, Czech Republic) equipped with a standard Everhart-Thornley secondary and scattered electron (SEM) and detector of backscat-

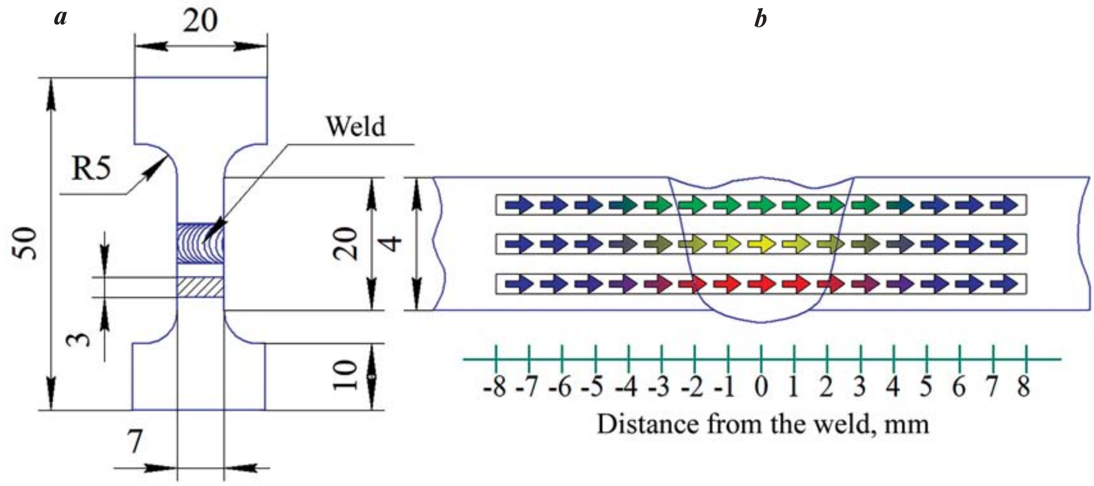

Fig. 2. Samples for uniaxial tensile tests: from VTI-4 plates after K-PAW (***a***); area for measuring microhardness in the cross section of a welded joint of the VTI-4 alloy (***b***)
The dimensions are specified in millimeters

Рис. 2. Образцы для испытаний на одноосное растяжение из пластин ВТИ-4 после плазменной сварки (***a***) и область измерения микротвердости в поперечном сечении сварного соединения (***b***)
Размеры указаны в мм

tered electron (BSE) at an accelerating voltage of 20—30 kV. EBSD analysis was performed in backscattered electron diffraction mode with grain orientation mapping. Samples for BSE analysis were fixed on an instrument table with a 45° tilt using carbon conductive adhesive 502 (EMS, USA) or clamps, while NEM TAPE carbon tape ("Nisshin", Japan) was used for ETD analysis. The sample, additionally tilted at a 25° angle (total angle of 70° to the horizontal), was scanned with a 3 μm step. Data processing and analysis were carried out using OIM Analysis 9 software (EDAX, USA).

Tensile tests on welded joints were conducted using a "5882 testing machine" (Instron, UK) at room temperature with a deformation rate of 10^{-4} s^{-1}. Control and data collection were performed using "Bluehill 2" software (Instron, UK). The scheme and dimensions of the samples for tensile testing are shown in Fig. 2, *a*. For testing, at least two samples of the base material, welded joints before and after heat treatment, were used.

Microhardness was determined on microgrinds in the cross-section of welded joints using a Vickers 402MVD microhardness tester (Netherlands) with a load of 200 g and an indentation time of 10 sec ($HV_{0.2}$) with a 0.2 mm step. Microhardness in the cross-section of the weld joint was evaluated at 3 points: in the area closer to the weld bead, in the middle of the weld joint, and closer to the weld root (Fig. 2, *b*). Control and data collection were performed using "Hardtest Wolpert Group" software (Netherlands).

Research results

The results of the study are presented in Table 1, which shows the tested parameters of keyhole plasma arc welding (K-PAW) for 4 mm thick plates made of the VTI-4 alloy. The selection of optimal K-PAW conditions was carried out on a control sample. It was found that at low currents, a melting channel is not formed, leading to disruption of the keyhole plasma arc welding process. Preliminary investigations showed that a high-quality welded joint was obtained with K-PAW in mode *4* (Table 2): the melting current of the keyhole was set at 160 A, the main welding current was 150 A, and the current at the end of welding was 20 A. In this case, the width of the weld bead is 6.0 mm, and the root of the weld is 3.0 mm. No external defects such as pores and cracks were observed in the resulting welded joints (Fig. 3). Thus, welded joints obtained in mode *4* were used for subsequent research.

Technological plates used for fixture fixation leave traces on the edges of the welded joint (Fig. 3). At the beginning of the weld, there is a zone with a buildup where through melting is formed, and at its end, a zone with edge melting is detected, formed as a result of the displacement of liquid metal to the newly melted weld pool. All detected defects are of a technological nature, which can be eliminated using fixating plates at the beginning and end of welding.

The cross-sectional structure of the welded joint, as determined by BSE-SEM analysis, is shown in Fig. 4. It exhibits an hourglass shape. Interestingly, the boundary of the fusion zone is less curved compared to welded joints after laser and electron beam welding (Fig. 4). This difference can be attributed to the plasma arc passing from top to bottom, resulting in a more evenly distributed heat across the cross-section of the central and root parts of the weld.

In the welded joint, three main zones can be distinguished: the weld zone or fusion zone (FZ), the heat-affected zone (HAZ), and the base metal (BM) (see Fig. 4—6). The fusion zone consists of large columnar β-phase dendrites oriented perpendicular to the fusion line (FL), with an average length of approximately ~750 μm (Fig. 6, *a*). According to EBSD analysis, large equiaxed crystals with a diameter of 350±50 μm were found in the middle of the weld, attributed to the larger volume of the liquid pool and reduced heat dissipation rate from the central part of the weld [23]. Due to the increased cooling rate, no formation of

Table 1. **The modes of keyhole plasma arc welding of the VTI-4 alloy plates with a thickness of 4 mm**

Таблица 1. Режимы плазменной сварки проникающей дугой пластин из сплава ВТИ-4 толщиной 4 мм

Mode number	Melting point of the lock bore, A	Main welding current, A	Current at the end of welding, A	Consumption of plasma-forming/protective gases, L/min
1	150	140	15	3/3
2	160	140	15	3/3
3	150	150	20	3/3
4	160	150	20	3/3

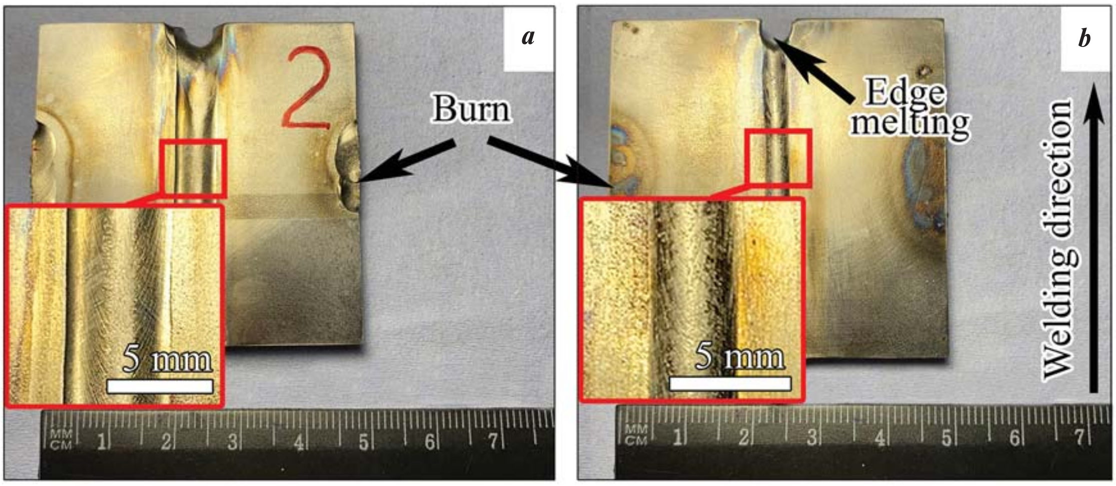

Fig. 3. Appearance of a welded joint of the VTI-4 alloy produced by K-PAW according to mode *4*
a – weld bead; ***b*** – root of the weld

Рис. 3. Внешний вид сварного соединения из сплава ВТИ-4, полученного плазменной сваркой проникающей дугой по режиму *4*
а – валик сварного шва; ***b*** – корень сварного шва

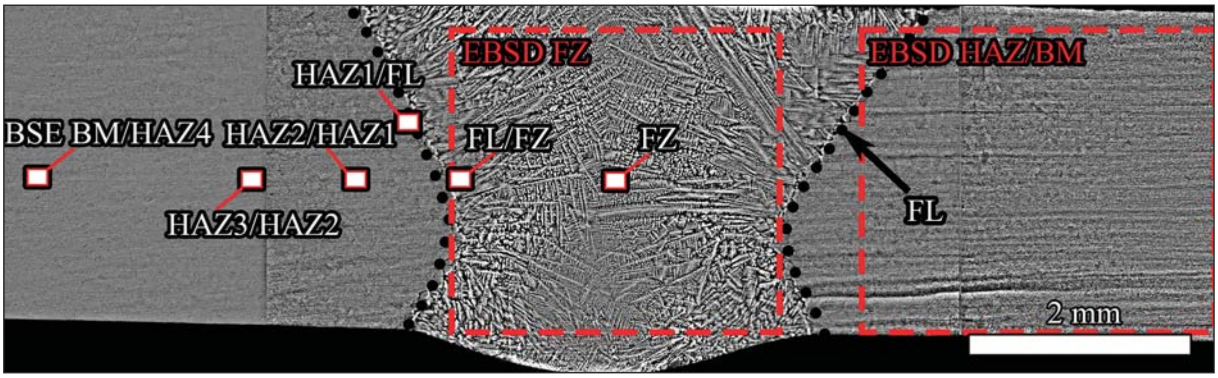

Fig. 4. Cross-section of a weld of the VTI-4 alloy produced by K-PAW with marking of areas for BSE and EBSD microstructural analysis, which are presented in Fig. 5 and 6, respectively

Рис. 4. Поперечное сечение сварного шва сплава ВТИ-4, полученного плазменной сваркой проникающей дугой, с разметкой областей съемки BSE- и EBSD-анализов (см. рис. 5 и 6)

Table 2. **Phase composition of the zones of the welded joint of the VTI-4 alloy obtained by K-PAW with subsequent heat treatment**

Таблица 2. Фазовый состав зон сварного соединения из сплава ВТИ-4, полученного плазменной сваркой проникающей дугой с последующей термической обработкой

Phases	Contentment, %					
	FZ	HAZ1	HAZ2	HAZ3	HAZ4	BM
α_2	–	<1	6.5	7.8	9.0	10.3
O	46.0	43.0	44.0	44.0	45.0	46.0
β	54.0	57.0	49.5	48.2	46.0	43.7

O- or α_2-phases occurs in the FZ [24]. Additionally, the high Nb content also contributes to the stabilization of the β-phase [25]. Internal pores were not detected in both the FZ and at the fusion line boundary (Fig. 5, *a*, *b*). In the near-fusion zone, large globular β-grains with an average size of ≈160±100 μm are formed along the fusion line. In the HAZ at a distance of 3.5±0.5 mm from the center of the weld, smaller equiaxed grains with an average size of ≈100±40 μm are observed (zone HAZ3, Fig. 6, *b*).

The structure of the HAZ after K-PAW can be divided into 4 zones depending on the phase composition and morphology. In the HAZ1 zone, close to the fusion line, large β-phase grains with diameters of 60—260 μm are observed (Fig. 5, *c*). Here, α_2- and

O-phases completely dissolved during the heating process of welding, and no reverse transformation occurred during cooling. In the HAZ2 and HAZ3 zones, the globular α_2-phase is partially preserved, as higher temperatures are required to complete the $\alpha_2 \rightarrow \beta$ transformation [25]. At the same time, large β-phase grains have sizes ranging from 40—160 μm (Fig. 5, *d*, *e*). HAZ4 consists of β-, O-, and α_2-phases (Fig. 5, *f*).

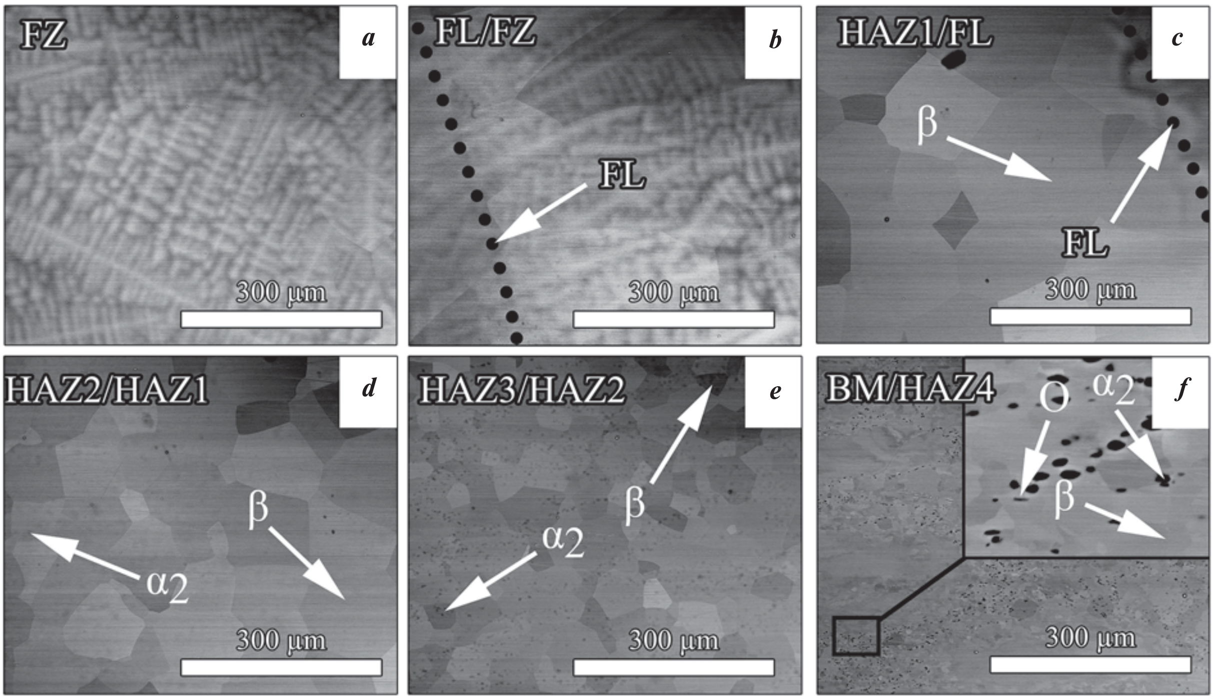

Fig. 5. BSE analysis of the microstructure in the cross section of the welded joint of the VTI-4 alloy produced by K-PAW

a – fusion zone (FZ); ***b*** – fusion line (FL); ***c*** – HAZ1; ***d*** – HAZ2; ***e*** – HAZ3; ***f*** – HAZ4 and base material (BM)

Рис. 5. Результаты BSE-анализа микроструктуры в поперечном сечении сварного соединения из сплава ВТИ-4, полученного плазменной сваркой проникающей дугой

a – зона плавления (ЗП); ***b*** – линия сплавления (ЛС); ***c*** – ЗТВ1; ***d*** – ЗТВ2; ***e*** – ЗТВ3; ***f*** – ЗТВ4 и основной материал (ОМ)

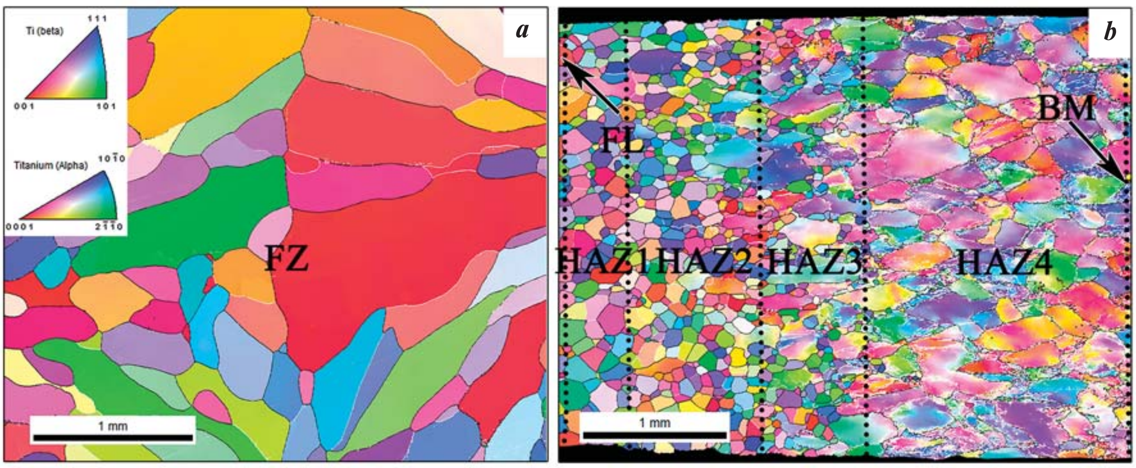

Fig. 6. EBSD analysis of a welded joint of VTI-4 alloy in the cross section of the weld obtained by K-PAW

a – center of the weld; ***b*** – from the fusion zone to the base metal

Рис. 6. EBSD-карты сварного соединения из сплава ВТИ-4 в поперечном сечении сварного шва, полученного плазменной сваркой проникающей дугой

a – центр сварного шва; ***b*** – участок от зоны плавления до основного металла

Unlike the BM, in HAZ4, during heating, the O-phase partially transforms into the β-phase, while the α_2-phase mainly remains.

The transition from HAZ2 to HAZ3 and HAZ4 is gradual and accompanied by the appearance of the α_2-phase and an increase in its proportion in the structure. During the transition from HAZ4 to BM, an increase in the O-phase content is observed. Zones of thermal influence with phase composition, morphology, and size similar to those described above were also observed in previous studies [25—27].

During the heat treatment process, within the fusion zone (FZ), needle-like O-phase particles with lengths ranging from 1.1—2.9 μm and thicknesses of 0.21±0.15 μm were precipitated (Fig. 7, *a*). In the HAZ1, precipitations of α_2-phase with sizes of 0.6±±0.2 μm formed along the boundaries of large β-grains, with an overall volume fraction not exceeding 1 %. Inside the β-grains, particles of the O-phase with lengths ranging from 0.8—2.1 μm were observed (Fig. 7, *b*). In the HAZ2, needle-like O-phase and α_2-phase precipitations were observed inside and along the boundaries of β-grains, respectively. Additionally, globular α_2-phase particles were found inside the β-grains (Fig. 7, *c*, *d*). In the HAZ4, particles of α_2-phase close to equiaxed shape with diameters of 0.7—3.5 μm, located along the boundaries of β-grains, and needle-like particles of the O-phase with lengths of 1.1—2.4 μm inside the β-grains were also observed (Fig. 7, *e*). In the base metal (BM) zone, a large number of globular α_2-phase particles with sizes ranging from 1.2—4.5 μm were present, predominantly along the boundaries of primary β-grains (Fig. 7, *f*). The BM zone differs from HAZ4 in its lower content of β-phase and higher content of O- and α_2-phases: 43.7 %, 46.0 %, and 10.3 %, respectively, compared to 46.0 %, 45.0 %, and 9.0 % in HAZ4.

The distribution of microhardness across the transverse section of the weld is shown in Fig. 8. The width of the fusion zone (FZ) ranges from 3 to 6 mm and is within the range of –3 to 3 mm on the graphs, with a microhardness of 360±15 $HV_{0.2}$. The heat-affected zone (HAZ) extends several millimeters on both sides, and the microhardness approaches the values of the base metal (BM) (420±15 $HV_{0.2}$). Thus, the width of the HAZ is 4—5 mm.

It is noteworthy that the microhardness profile at dif-

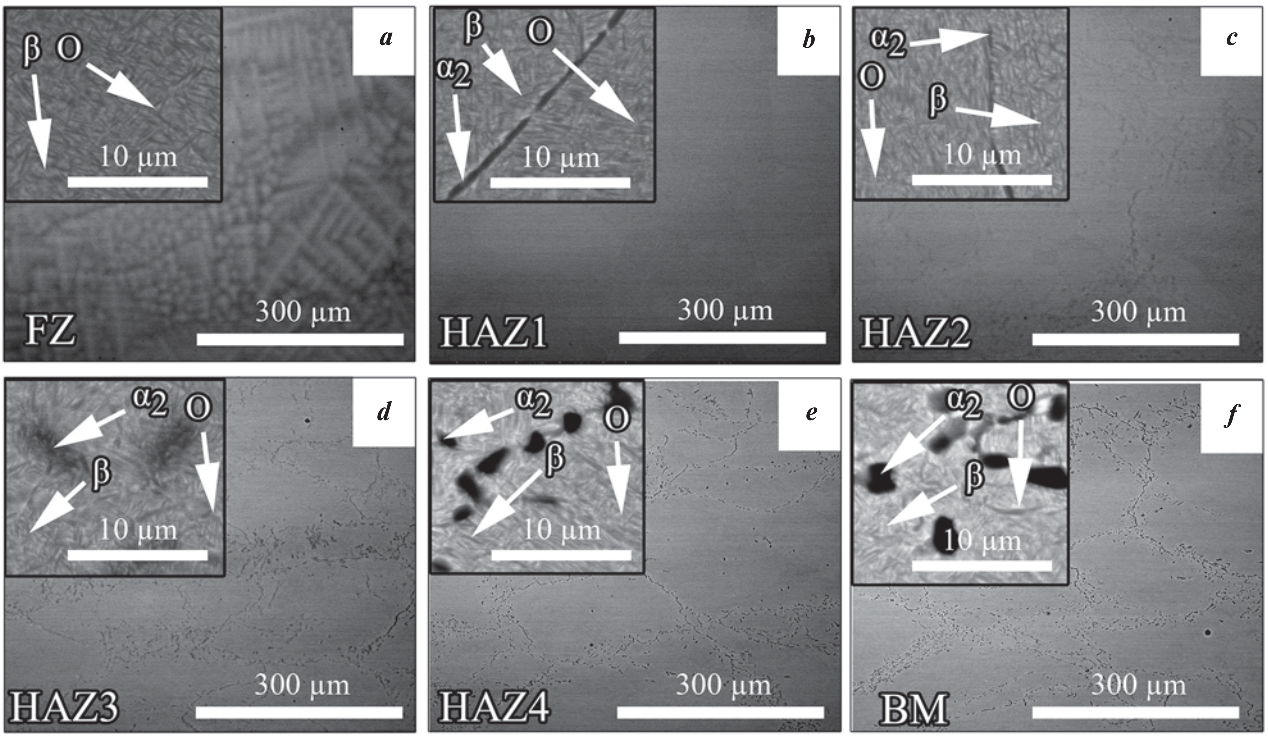

Fig. 7. The results of the BSE analysis of the microstructure in the cross-section of the welded joint of the VTI-4 alloy, obtained by K-PAW followed by heat treatment

a – fusion zone (FZ); ***b*** – HAZ1; ***c*** – HAZ2; ***d*** – HAZ3; ***e*** – HAZ4; ***f*** – base metal (BM)

Рис. 7. Результаты BSE-анализа микроструктуры в поперечном сечении сварного соединения из сплава ВТИ-4, полученного плазменной сваркой проникающей дугой с последующей термической обработкой

a – зона плавления (ЗП); ***b*** – ЗТВ1; ***c*** – ЗТВ2; ***d*** – ЗТВ3; ***e*** – ЗТВ4; ***f*** – основной металл (ОМ)

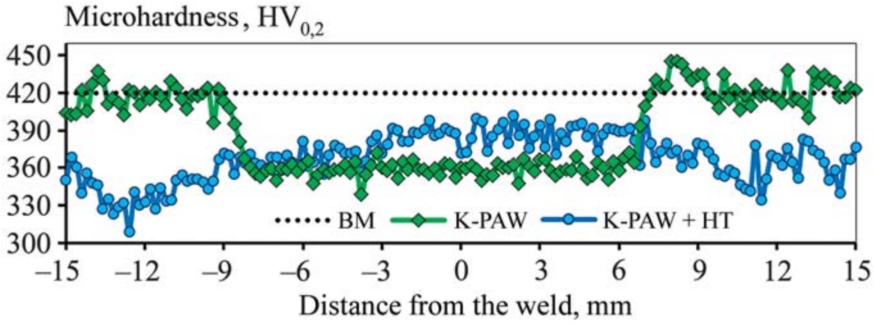

Fig. 8. Microhardness of the initial plate ($HV_{0.2}$ BM) and welded joints of the VTI-4 alloy in the cross section of the weld obtained by K-PAW ($HV_{0.2}$ K-PAW) with subsequent heat treatment ($HV_{0.2}$ K-PAW + HT) [K-PAW – keyhole plasma arc welding, HT – heat treatment]

Рис. 8. Усредненные значения микротвердости исходной заготовки (ОМ) и сварных соединений из сплава ВТИ-4 в поперечном сечении сварного шва, полученных плазменной сваркой проникающей дугой (ПС) с последующей термической обработкой (ПС + ТО)

ferent levels of the weld remains nearly the same. It is known [28] that for Ti_2AlNb alloys, dispersion strengthening of the O-phase is the main strengthening mechanism. Therefore, due to the absence of the O-phase, the microhardness is lowest in the FZ and HAZ1 immediately after welding. However, as the transition from the FZ to the BM occurs, it increases [29].

After heat treatment (quenching + aging), the microhardness level slightly increases in the FZ and HAZ1 to 382±20 $HV_{0.2}$ (Fig. 8). At the same time, a decrease in microhardness to 310—380 $HV_{0.2}$ is observed in HAZ3 and the BM. The hardness profile is closely related to the structural state in each zone. The increase in microhardness in the FZ is primarily associated with the precipitation of fine O-phase during heat treatment [24; 28]. However, a noticeable decrease in microhardness was observed in the BM and HAZ4, which can be explained by the softening effect of static recovery and recrystallization [30].

The tensile test diagrams of samples cut from the original forged blank, as well as the welded joint before and after heat treatment (HT), are presented in Fig. 9. The mechanical properties of the welded joint without HT are at a level higher than 80 % of the parameters of the original blank (σ_{ucs} = 1020 MPa, σ_{ys} = = 1010 MPa); however, elongation to failure of the weld is substantially lower (0.5 %), which may be attributed to the formation of large dendrites of the β-phase in the fusion zone (FZ) [31]. The mechanical properties of the welded joint after HT reach a level exceeding 90 % of the initial state (σ_{ucs} = 1120 MPa, σ_{ys} = 1090 MPa). Thus, heat treatment contributes to an increase in mechanical properties by approximately 10 % compared to welded joints obtained under plasma welding conditions without subsequent heat treatment. At the same time, elongation to failure of the welded joint reached 2.1 %.

Fracture of the base metal after tensile testing mostly exhibits a ductile relief; however, zones of ductile failure with the formation of dimples and quasi-brittle cleavage facets are identified, explaining the higher ductility of the material (Fig. 10, *c*, *d*). In the welded joint, failure occurs through the FZ, and a ductile relief is observed on the fracture surface (Fig. 10, *a*, *b*). Microcracks and pores, which could have opened up or become place of failure, were not detected.

The observed fracture is characteristic of welds with a β-phase structure [24; 25], where fracture involves the splitting of the crack at the base of the ductile pattern. In this case, transgranular brittle fracture explains the low ductility of the material [31]. Welded joints after HT fail through a mixed mechanism of inter- and transgranular fracture (Fig. 10, *e*—*h*).

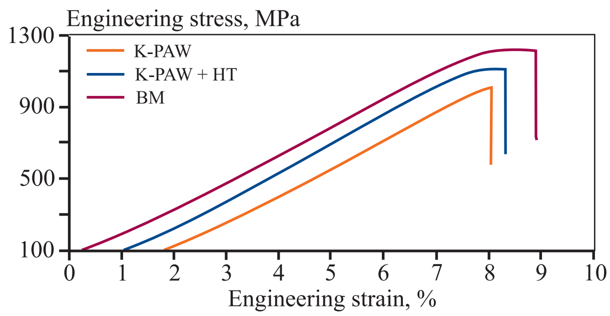

Fig. 9. Tensile diagram of the base metal (BM), welded joint (K-PAW) of the VTI-4 alloy with subsequent heat treatment (K-PAW + HT) obtained by K-PAW

Рис. 9. Диаграммы растяжения основного металла (ОМ), сварного соединения (ПС) из сплава ВТИ-4, полученного плазменной сваркой с последующей термической обработкой (ПС + ТО)

The fracture occurs at the boundary (fusion line) between the weld and the HAZ1. Obviously, the precipitation of the O-phase in the FZ contributed to the strengthening of the weld, and failure occurred at the FZ/HAZ1 interface. Cracks along the boundaries of large β-phase grains are observed on the fracture surface (Fig. 10, *g*, *h*), as well as facets of transgranular fracture.

Thus, compared to TIG welding of Ti_2AlNb-based alloys [8; 32], keyhole plasma arc welding maintains a large dendritic structure in the weld, but due to the increased thickness of the welded metal and welding speed, the productivity of the process for producing non-detachable joints significantly increases. Furthermore, after heat treatment (HT), the mechanical properties of the welded joints reach levels close to those of the base metal (>90 %).

In comparison to laser beam welding of VT1-4 titanium aluminide-based alloys, which are similar in structure and properties to the original blanks [15],

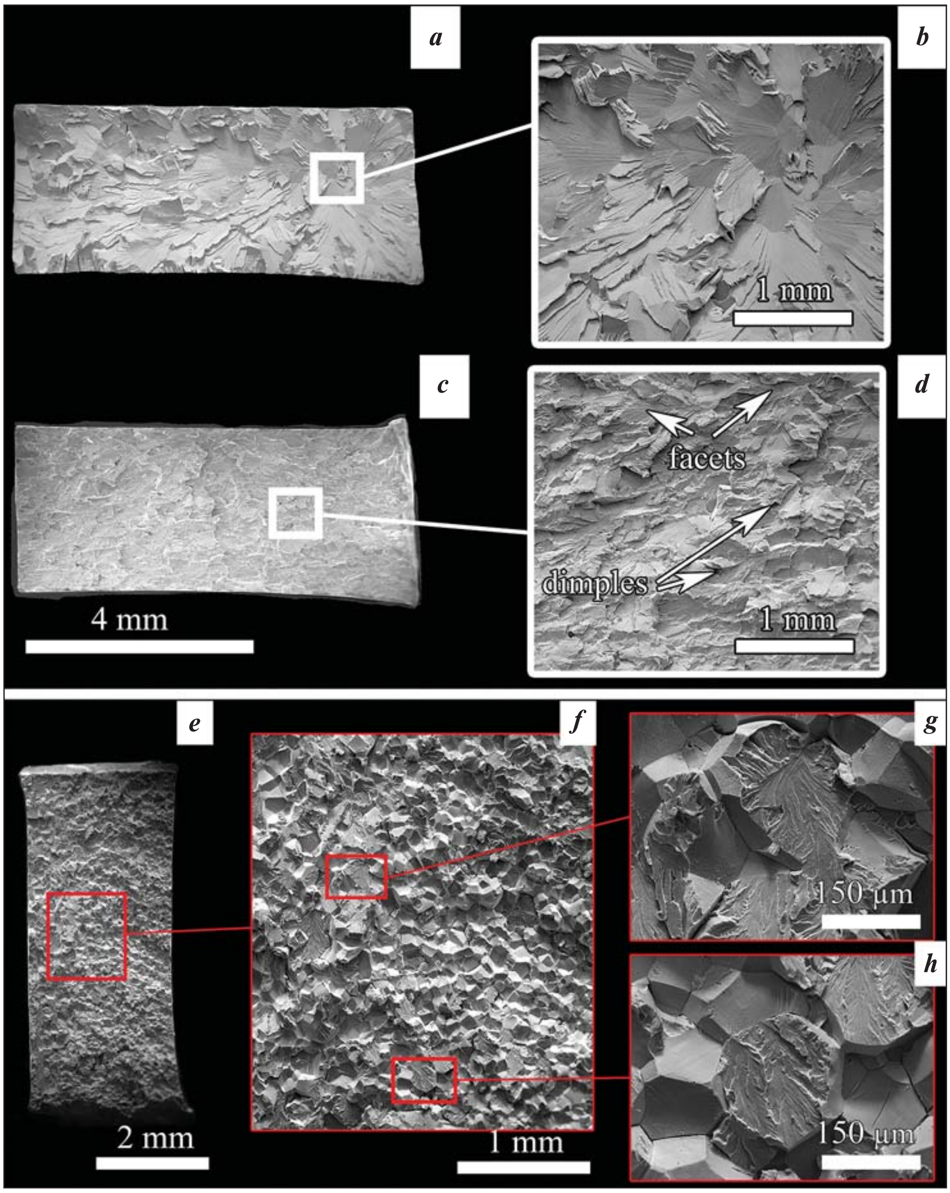

Fig. 10. Morphology of fracture surface of samples after tensile tests: ***a*** – general view of the fracture of the welded joint (WJ); ***b*** – morphology of the fracture surface of the WJ; ***c*** – general view of the fracture of the base metal (BM); ***d*** – morphology of the fracture surface of the BM; ***e*** – general view of the fracture of the WJ after heat treatment (HT); ***f–h***– morphology of the fracture surface of the WJ after HT

Рис. 10. Поверхности разрушения образцов после испытаний на растяжение: общий вид и микростроение изломов сварного соединения (***a***, ***b***), основного металла (***c***, ***d***) и сварного соединения после термообработки (***e–h***)

K-PAW ensures the absence of porosity in the weld due to the specific dynamic impact of the plasma arc during welding. Despite the large dendritic structure of the weld after K-PAW (~750 μm), the level of mechanical properties of such dense, defect-free (no porosity) welded joints is close to that of welds obtained by pulsed laser beam welding [15].

Conclusion

Within the scope of this study, the keyhole plasma arc welding (K-PAW) mode for 4 mm thick plates made of VT1-4 alloy was determined to achieve defect-free welded joints, consisting of the fusion zone, heat-affected zone, and base metal. The HAZ structure after welding, depending on the phase composition and morphology of the phases, can be divided into the following zones: HAZ1 — zone of large β-phase grains near the fusion line; HAZ2 — zone of large β-phase grains with α_2-phase particles; HAZ3 — zone with more fragmented β-phase grains with a large amount of α_2-phase preserved; HAZ4 — zone containing β-, α_2-, and O-phases.

The microhardness of the weld in the FZ corresponds to 360±15 $HV_{0.2}$, and after heat treatment (HT) (quenching at t = 920 °C, holding for 2 h, air cooling, aging at 800 °C, τ = 6 h, air cooling), it increases to 382±20 HV0.2 due to strengthening from the precipitation of fine O-phase particles. The mechanical properties of the welded joint after HT are above 90 % of the parameters of the original forged blank (σ_{ucs} = 1120 MPa, σ_{ys} = 1090 MPa), with elongation to failure approaching the original state (δ = = 2.1 %).

References

1. Goyal K., Bera C., Sardana N. Temperature-dependent structural, mechanical, and thermodynamic properties of B2-phase Ti_2AlNb for aerospace applications. *Journal of Materials Science*. 2022;57(41):19553—19570. https://doi.org/10.1007/s10853-022-07788-3
2. Shagiev M.R., Galeyev R.M., Valiakhmetov O.R. Ti_2AlNb-Based intermetallic alloys and composites. *Materials Physics and Mechanics*. 2017;33(1):12—18. https://doi.org/10.18720/MPM.3312017_2
3. Nandy T.K., Banerjee D. Creep of the orthorhombic phase based on the intermetallic Ti_2AlNb. *Intermetallics*. 2000;8(8):915—928. https://doi.org/10.1016/S0966-9795(00)00059-5
4. Emura S., Araoka A., Hagiwara M. B2 grain size refinement and its effect on room temperature tensile properties of a Ti—22Al—27Nb orthorhombic intermetallic alloy. *Scripta Materialia*. 2003;48:629—634. https://doi.org/10.1016/S1359-6462(02)00462-1
5. Kim Y.-W., Dimiduk D.M. Progress in the understanding of gamma titanium aluminides. *Journal of Minerals, Metals & Materials Society*. 1991;43:40—47. https://doi.org/10.1007/BF03221103
6. Kumpfert J., Leyens C. Orthorhombic titanium aluminides: Intermetallics with improved damage tolerance. In: *Titanium and Titanium Alloys — Fundamentals and Applications*. GmbH & Co.: Wiley—VCH Verlag, 2005. P. 59—88. https://doi.org/10.1002/3527602119.ch3
7. Li Y.-J., Wu A.-P., Li Q., Zhao Y., Zhu R.-C., Wang G.-Q. Effects of welding parameters on weld shape and residual stresses in electron beam welded Ti_2AlNb alloy joints. *Transactions of Nonferrous Metals Society of China*. 2019;29(1):67—76. https://doi.org/10.1016/S1003-6326(18)64916-7
8. Liu X., Shao L., Ji Y., Zhao H., Wan X. Ultrasonic frequency pulse tungsten inert gas welding of Ti_2AlNb-based alloy. *Chinese Journal of Rare Metals*. 2014;38(4): 541—547. https://doi.org/10.13373/j.cnki.cjrm.2014.04.001
9. Shao L., Wu S., Datye A., Zhao H., Petterson M., Peng W. Microstructure and mechanical properties of ultrasonic pulse frequency tungsten inert gas welded Ti—22Al—25Nb (at.%) alloy butt joint. *Journal of Materials Processing Technology*. 2018;259:416—423. https://doi.org/10.1016/j.jmatprotec.2018.03.018
10. Bu Z., Ma X., Li R., Wu J., Li J. Effect of pressure on microstructure and mechanical properties of diffusion bonded joints of Ti_2AlNb alloy. *Journal of Aeronautical Materials*. 2023;43:51—58. https://doi.org/10.11868/j.issn.1005-5053.2022.000162
11. Niu T., Jiang B., Zhang N., Wang Y. Microstructure and mechanical properties of Ti—Ti_2AlNb interface. *Composites and Advanced Materials*. 2021;30:1—7. https://doi.org/10.1177/2633366X20929
12. Chen X., Zhang Z., Xie F., Wu X., Ma T., Li W., Sun D. Optimizing the integrity of linear friction welded Ti_2AlNb alloys. *Metals*. 2021;11(5):802. https://doi.org/10.3390/met11050802
13. Cui D., Wu Q., Jin F., Xu C., Wang M., Wang Z., Li J., He F., Li J., Wang J. Heterogeneous deformation behaviors of an inertia friction welded Ti_2AlNb joint: an in-situ study. *Acta Metallurgica Sinica*. 2023;36(4):611—622. https://doi.org/10.1007/s40195-022-01477-5
14. Panov D., Naumov S., Stepanov N., Sokolovsky V., Volokitina E., Kashaev N., Ventzke V., Dinse R., Riekehr S., Povolyaeva E., Nochovnaya N., Alekseev E., Zherebtsov S., Salishchev G. Effect of pre-heating and post-weld heat treatment on structure and mechanical properties of

laser beam-welded Ti_2AlNb-based joints. *Intermetallics*. 2022;143:107466.
https://doi.org/10.1016/j.intermet.2022.107466

15. Naumov S.V., Panov D.O., Chernichenko R.S., Sokolovsky V.S., Volokitina E.I., Stepanov N.D., Zherebtsov S.V., Alekseev E.B., Nochovnaya N.A., Salishchev G.A. Structure and mechanical properties of welded joints from alloy based on VTI-4 orthorhombic titanium aluminide produced by pulse laser welding. *Izvestiya. Non-Ferrous Metallurgy*. 2023;29(2):57—73.
https://doi.org/10.17073/0021-3438-2023-2-57-73
Наумов С.В., Панов Д.О., Черниченко Р.С., Соколовский В.С., Волокитина Е.И., Степанов Н.Д., Жеребцов С.В., Алексеев Е.Б., Ночовная Н.А., Салищев Г.А. Структура и механические свойства сварных соединений из сплава на основе орторомбического алюминида титана ВТИ-4, полученных импульсной лазерной сваркой. *Известия вузов. Цветная металлургия*. 2023;29(2):57—73.
https://doi.org/10.17073/0021-3438-2023-2-57-73
16. Lei Z., Zhang K, Zhou H., Ni L., Chen Y. A comparative study of microstructure and tensile properties of Ti_2AlNb joints prepared by laser welding and laser-additive welding with the addition of filler powder. *Journal of Materials Processing Technology*. 2018;255:477—487.
https://doi.org/10.1016/j.jmatprotec.2017.12.044
17. Bu Z., Wu J., Ma X., Li Z., Li J. Microstructure and mechanical properties of electron beam welded joints of Ti_2AlNb alloy. *Journal of Materials Engineering and Performance*. 2022;20:5329—5337.
https://doi.org/10.1007/s11665-022-07514-9
18. Li L., Fu P., Zhao T., Tang Z., Mao Z. Effect of preheating on the microstructure evolution and mechanical properties of electron beam welded Ti_2AlNb alloy. *Journal of Materials Engineering and Performance*. 2022;32(8): 3648—3657. https://doi.org/10.1007/s11665-022-07346-7
19. Li Y., Zhao Y., Li Q., Wu A., Zhu R., Wang G. Effects of welding condition on weld shape and distortion in electron beam welded Ti_2AlNb alloy joints. *Materials & Design*. 2017;114:226—233.
https://doi.org/10.1016/j.matdes.2016.11.083
20. Short A.B. Gas tungsten arc welding of $\alpha + \beta$ titanium alloys: A review. *Materials Science and Technology*. 2009;25(3):309—324.
https://doi.org/10.1179/174328408X389463
21. Li Z., Cui Y., Yu Z., Liu C. In-situ fabrication of Ti_2Al-Nb-based alloy through double-wire arc additive manufacturing. *Journal of Alloys and Compounds*. 2021;876: 160021. https://doi.org/10.1016/j.jallcom.2021.160021
22. Shchitsyn Yu.D., Tytkin Yu.M. Interaction of a compressed arc with a crater cavity during keyhole plasma arc welding. *Svarochnoe proizvodstvo*. 1994;6:32—33. (In Russ.).
Щицын Ю.Д., Тыткин Ю.М. Взаимодействие сжатой дуги с полостью кратера при плазменной сварке проникающей дугой. *Сварочное производство*. 1994;6:32—33.
23. Stefanescu D.M., Ruxanda R. Solidification structures of titanium alloys. In: *ASM Handbook Metallography and Microstructures*. 2004. P. 116—126.
https://doi.org/10.31399/asm.hb.v09.a0003728
24. Wu J. Xu L., Lu Z., Cui Y., Yang R. Preparation of powder metallurgy Ti—22Al—24Nb—0.5Mo alloys and electron beam welding. *Acta Metallurgica Sinica*. 2016;52(9): 1070—1078.
https://doi.org/10.11900/0412.1961.2016.00019
25. Zhang K., Lei Z., Chen Y., Yang K., Bao Y. Heat treatment of laser-additive welded Ti_2AlNb joints: Microstructure and tensile properties. *Materials Science and Engineering: A*. 2019;744:436—444.
https://doi.org/10.1016/j.msea.2018.12.058
26. Zhang K., Ni L., Lei Z., Chen Y., Hu X. Microstructure and tensile properties of laser welded dissimilar Ti—22Al—27Nb and TA15 joints. *The International Journal of Advanced Manufacturing Technology*. 2016;87:1685—1692.
https://doi.org/10.1007/s00170-016-8579-3
27. Wang L., Sun D., Li H., Gu X., Shen C. Microstructures and mechanical properties of a laser-welded joint of Ti_3Al—Nb alloy using pure Nb filler metal. *Metals*. 2018;8(10):785. https://doi.org/10.3390/met8100785
28. Chen X., Xie F.Q., Ma T.J., Li W.Y., Wu X.Q. Effects of post-weld heat treatment on microstructure and mechanical properties of linear friction welded Ti_2AlNb alloy. *Materials & Design*. 2016;94:45—53.
https://doi.org/10.1016/j.matdes.2016.01.017
29. Chen W., Chen Z.Y., Wu C.C., Li J.W., Tang Z.Y., Wang Q.J. The effect of annealing on microstructure and tensile properties of Ti—22Al—25Nb electron beam weld joint. *Intermetallics*. 2016;75:8—14.
https://doi.org/10.1016/j.intermet.2016.02.006
30. Jiao X., Kong B., Tao W., Liu G., Ning H. Effects of annealing on microstructure and deformation uniformity of Ti—22Al—24Nb—0.5Mo laser-welded joints. *Materials & Design*. 2017;130:166—174.
https://doi.org/10.1016/j.matdes.2017.05.005
31. Lei Z., Zhou H., Chen Y., Zhang K., Li B. A comparative study of deformation behaviors between laser-welded joints and base metal of Ti—22Al—24.5Nb—0.5Mo alloy. *Journal of Materials Engineering and Performance*. 2019;28(8):5009—5020.
https://doi.org/10.1007/s11665-019-04224-7
32. Lu B., Yin J., Wang Y., Yang R. Gas tungsten arc welding of Ti_2AlNb based alloy sheet. In: *Proc. 12th World Conf. Titan* (China, Beijing, 19—24 June 2011). 2012. Vol. 1. P. 816—818.

Information about the authors

Stanislav V. Naumov – Cand. Sci. (Eng.), Associate Professor of the Department of Materials Science and Nanotechnology (MSN), Senior Research Scientist of the Laboratory of Bulk Nanostructured Materials (BNM), Belgorod National Research University (BSU).
https://orcid.org/0000-0002-4084-8861
E-mail: NaumovStanislav@yandex.ru

Dmitrii O. Panov – Cand. Sci. (Eng.), Associate Professor of the Department MSN, Senior Research Scientist of the Laboratory BNM, BSU.
https://orcid.org/0000-0002-8971-1268
E-mail: dimmak-panov@mail.ru

Ruslan S. Chernichenko – Junior Researcher of the Laboratory BNM, BSU.
https://orcid.org/0000-0002-8619-0700
E-mail: chernichenko@bsu.edu.ru

Vitaly S. Sokolovsky – Cand. Sci. (Eng.), Research Scientist of the Laboratory BNM, BSU.
https://orcid.org/0000-0001-5607-2765
E-mail: sokolovskiy@bsu.edu.ru

Gennady A. Salishchev – Dr. Sci. (Eng.), Professor of the Department MSN, Head of the Laboratory BNM, BSU.
https://orcid.org/0000-0002-0815-3525
E-mail: salishchev_g@bsu.edu.ru

Evgeny B. Alekseev – Cand. Sci. (Eng.), Head of the Sector of All-Russia Institute of Aviation Materials of the National Research Center "Kurchatov Institute".
Scopus-ID: 56581528500
E-mail: hiten_@mail.ru

Sergey D. Neulybin – Cand. Sci. (Eng.), Head of the Laboratory of methods for creating and designing systems "Material–Technology–Design", Perm National Research Polytechnic University (PNRPU).
https://orcid.org/0000-0003-1846-1502
E-mail: sn-1991@mail.ru

Dmitry S. Belinin – Cand. Sci. (Eng.), Associate Prof. of the Department of Welding, Metrology and Materials Engineering (WMME), PNRPU.
https://orcid.org/0000-0001-5462-0908
E-mail: 5ly87@mail.ru

Yuri D. Shchitsyn – Dr. Sci. (Eng.), Professor, Head of the Department WMME, PNRPU.
https://orcid.org/0000-0002-3499-4184
E-mail: schicin@pstu.ru

Vasily V. Lukianov – Cand. Sci. (Eng.), Head of the Department of Complex-Profile Shaping, NPA "Technopark AT".
https://orcid.org/0009-0006-3621-3966
E-mail: lukianovv@bk.ru

Информация об авторах

Станислав Валентинович Наумов – к.т.н., доцент кафедры материаловедения и нанотехнологий (МиН), ст. науч. сотрудник лаборатории объемных наноструктурных материалов (ОНМ), Белгородский государственный национальный исследовательский университет (НИУ «БелГУ»).
https://orcid.org/0000-0002-4084-8861
E-mail: NaumovStanislav@yandex.ru

Дмитрий Олегович Панов – к.т.н., доцент кафедры МиН, ст. науч. сотрудник лаборатории ОНМ, НИУ «БелГУ».
https://orcid.org/0000-0002-8971-1268
E-mail: dimmak-panov@mail.ru

Руслан Сергеевич Черниченко – мл. науч. сотрудник лаборатории ОНМ, НИУ «БелГУ».
https://orcid.org/0000-0002-8619-0700
E-mail: chernichenko@bsu.edu.ru

Виталий Сергеевич Соколовский – к.т.н., науч. сотрудник лаборатории ОНМ, НИУ «БелГУ».
https://orcid.org/0000-0001-5607-2765
E-mail: sokolovskiy@bsu.edu.ru

Геннадий Алексеевич Салищев – д.т.н., профессор кафедры МиН, зав. лабораторией ОНМ, НИУ «БелГУ».
https://orcid.org/0000-0002-0815-3525
E-mail: salishchev_g@bsu.edu.ru

Евгений Борисович Алексеев – к.т.н., начальник сектора Всероссийского научно-исследовательского института авиационных материалов Национального исследовательского центра «Курчатовский институт».
Scopus-ID: 56581528500
E-mail: hiten_@mail.ru

Сергей Дмитриевич Неулыбин – к.т.н., руководитель лаборатории методов создания и проектирования систем «Материал–Технология–Конструкция», Пермский национальный исследовательский политехнический университет (ПНИПУ).
https://orcid.org/0000-0003-1846-1502
E-mail: sn-1991@mail.ru

Дмитрий Сергеевич Белинин – к.т.н., доцент кафедры сварочного производства, метрологии и технологии материалов (СПМТМ), ПНИПУ.
https://orcid.org/0000-0001-5462-0908
E-mail: 5ly87@mail.ru

Юрий Дмитриевич Щицын – д.т.н., профессор, зав. кафедрой СПМТМ, ПНИПУ.
https://orcid.org/0000-0002-3499-4184
E-mail: schicin@pstu.ru

Василий Васильевич Лукьянов – к.т.н., начальник отдела сложнопрофильного формообразования, НПА «Технопарк АТ».
https://orcid.org/0009-0006-3621-3966
E-mail: lukianovv@bk.ru

Contribution of the authors

S.V. Naumov – formation of the main concept, planning and conducting experiments, writing the text, formulation of the conclusions.

D.O. Panov – organization and conducting of microstructural studies, writing the text, correction of the text and conclusions.

R.S. Chernichenko – carrying out mechanical tests of samples, analysis of the research results.

V.S. Sokolovsky – preparing samples for experiments, conducting EBSD analysis.

G.A. Salishchev – scientific guidance, goal and objectives of the study, participating in the discussion of the results, correcting the article.

E.B. Alekseev – producing the initial alloy for experiments.

S.D. Neulybin – management and conducting of welding studies, participating in the discussion of the results, correction of the text.

D.S. Belinin – preparing samples and conducting of welding studies.

Yu.D. Shchitsyn – provision of the resources, participating in the discussion of the welding results.

V.V. Lukianov – provision of the resources, planning experiments.

Вклад авторов

С.В. Наумов – формирование основной концепции, планирование и проведение экспериментальных работ, подготовка текста, формулировка выводов.

Д.О. Панов – организация и проведение микроструктурных исследований, подготовка текста статьи, корректировка выводов.

Р.С. Черниченко – проведение механических испытаний образцов, анализ результатов исследований.

В.С. Соколовский – подготовка образцов для экспериментов, проведение EBSD-анализа.

Г.А. Салищев – научное руководство, постановка цели и задач работы, участие в обсуждении результатов, правка статьи.

Е.Б. Алексеев – изготовление исходного сплава для экспериментов.

С.Д. Неулыбин – руководство и проведение сварочно-технологических работ, участие в обсуждении результатов, корректировка текста статьи.

Д.С. Белинин – подготовка образцов и проведение сварочно-технологических работ.

Ю.Д. Щицын – обеспечение ресурсами, участие в обсуждении результатов сварочно-технологических работ.

В.В. Лукьянов – обеспечение ресурсами, планирование экспериментальных работ.

The article was submitted 20.12.2023, revised 28.01.2024, accepted for publication 01.02.2024

Статья поступила в редакцию 20.12.2023, доработана 28.01.2024, подписана в печать 01.02.2024